Mechanical properties of amorphous nanosprings

INSTITUTE OF PHYSICS PUBLISHING NANOTECHNOLOGY
Nanotechnology **17** (2006) 5620–5626 doi:10.1088/0957-4484/17/22/015

Mechanical properties of amorphous nanosprings

Alexandre F da Fonseca[1], C P Malta[1] and D S Galvão[2]

[1] Instituto de Física, Universidade de São Paulo, Caixa Postal 66318, 05315-970, São Paulo, Brazil
[2] Instituto de Física 'Gleb Wataghin', Universidade Estadual de Campinas, Unicamp 13083-970, Campinas, SP, Brazil

E-mail: afonseca@if.usp.br, coraci@if.usp.br and galvao@ifi.unicamp.br

Received 11 July 2006, in final form 12 September 2006
Published 26 October 2006
Online at stacks.iop.org/Nano/17/5620

Abstract
Helical amorphous nanosprings have attracted particular interest due to their special mechanical properties. In this work we present a simple model, within the framework of the Kirchhoff rod model, for investigating the structural properties of nanosprings having asymmetric cross section. We have derived expressions that can be used to obtain the Young's modulus and Poisson's ratio of the nanospring material composite. We also address the importance of the presence of a catalyst in the growth process of amorphous nanosprings in terms of the stability of helical rods.

1. Introduction

Helical nanowires, or simply *nanosprings*, are particularly interesting one-dimensional nanostructures [1] due to their special periodic and elastic properties. Examples of such structures are quasi-nanosprings [2], helical crystalline nanowires [3–5] and amorphous nanosprings [6–8].

Volodin *et al* [9] have studied the elastic properties of helix-shaped nanotubes using atomic force microscopy (AFM). They used a circular beam approximation to model the elastic response of a single winding of a coiled nanotube. Recently, Chen *et al* [10] measured the spring constant of carbon nanocoils and used a classical approach which relates the spring constant to the shear modulus of the composite material.

In this paper, we present a model that can be used by experimentalists to determine the elastic properties of different amorphous nanosprings. Our calculations are based on the Kirchhoff rod model [11] that provides a framework for studying the statics and dynamics of thin elastic filaments. The static Kirchhoff equations will be used to derive expressions for the Young's modulus and the Poisson's ratio of the nanospring material composite. The nanowire here is assumed to have elliptic cross section, so the present work constitutes an extension of our previous works [12, 13] for nanowires with circular cross section.

It is known that the synthesis of amorphous nanowires and nanosprings requires the presence of a metallic catalyst. Following the vapour–liquid–solid (VLS) growth model, known since 1964 [14] for whisker formation, a liquid droplet of a metal absorbs a given material from the surrounding vapour, and after supersaturation of the absorbed material within the droplet, the excess material precipitates at the liquid–solid interface forming the nanowire beneath the metallic droplet.

McIlroy *et al* [1, 6] developed a modified VLS growth model to explain the formation of amorphous nanosprings based on the interactions between the metallic catalyst and the nanowire. The interesting feature is that the modified VLS growth model [1] does not depend on the composite material of the nanospring and, therefore, it can be applied to any type of amorphous nanospring.

Here, we will take advantage of the modified VLS growth model proposed by McIlroy *et al* [1] to analyse an important mechanical consequence of the presence of the metallic catalyst in the growth process of amorphous nanosprings. We show that the asymmetric growth driven by the metallic catalyst provides the nanowire with a *helical intrinsic curvature* which is required to maintain it to be dynamically stable.

The Kirchhoff model [11] has been extensively used to model the structure and elasticity of long DNA chains [15–21], the tendrils of climbing plants [22, 23], slender cables subject to different stresses [24], etc. The Kirchhoff model is also appropriate for investigating the elastic properties of amorphous helical nanostructures.

For nanowires with elliptic cross section, there are two types of helical structure, *normal* and *binormal*. In section 2, we present the Kirchhoff rod model and, for each type of helix, derive two expressions that can be used to obtain the Young's modulus and the Poisson's ratio of an amorphous nanospring composite material. One of the expressions relates the Hooke's constant to the Young's modulus, and to the geometric features of the nanospring. The other expression relates an applied torque in the direction of the helical axis of the nanospring to the Young's modulus and Poisson's ratio of the material. In section 3, we use the measured Hooke's constant for a carbon nanocoil, reported in [10], to test the expression for the Young's modulus. We discuss the results and analyse the stability of helical filaments, showing that the presence of a metallic catalyst has important consequences in the growth process of nanosprings. In section 4 we summarize our results and conclusions.

2. The elastic model

In this section, we derive two expressions that can be used by experimentalists to obtain the elastic constants of the composite material of amorphous nanosprings. Both expressions involve two geometric parameters that define a helical space curve, namely, the *curvature*, κ, and the *torsion*, τ.

We shall first briefly describe a helical curve and its relation to the curvature and torsion. Then, we present the Kirchhoff rod model that is used to derive the above-mentioned expressions for studying the elastic properties of amorphous nanosprings.

2.1. Helical space curve

A space curve $\mathbf{x}$ is a *helix* if the lines tangent to $\mathbf{x}$ make a constant angle with a fixed direction in space (the helical axis) [25].

A helical space curve $\mathbf{x}$ can be expressed in a fixed Cartesian basis as

$$\mathbf{x} = R\cos(\lambda s)\,\mathbf{e}_x + R\sin(\lambda s)\,\mathbf{e}_y + \frac{P}{2\pi}\lambda s\,\mathbf{e}_z, \tag{1}$$

where

$$\lambda = \sqrt{\frac{1}{(R^2 + \frac{P^2}{4\pi^2})}}, \tag{2}$$

R is the radius of the helix, and P is the *pitch* of the helix, i.e., the distance between two adjacent loops. $\{\mathbf{e}_x, \mathbf{e}_y, \mathbf{e}_z\}$ is a fixed Cartesian basis, where $\mathbf{e}_z$ is chosen along the direction of the axis of the helix. Figure 1 shows a helical filament of radius R, and pitch P.

The radius, R, and pitch, P, of the helix are related to the curvature, κ, and torsion, τ, through

$$\kappa = R\lambda^2, \qquad \tau = \frac{P}{2\pi}\lambda^2. \tag{3}$$

In terms of κ and τ, the helical curve $\mathbf{x}$ can be written as [23]

$$\mathbf{x} = \frac{\kappa}{\lambda^2}\cos(\lambda s)\,\mathbf{e}_1 + \frac{\kappa}{\lambda^2}\sin(\lambda s)\,\mathbf{e}_2 + \frac{\tau}{\lambda}s\,\mathbf{e}_3, \tag{4}$$

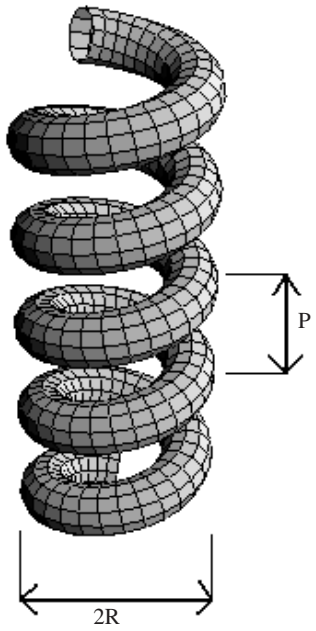

Figure 1. A helical rod characterized by a radius R and a loop-to-loop distance P.

where λ can also be written in terms of κ and τ by

$$\lambda = \sqrt{\kappa^2 + \tau^2}. \tag{5}$$

These equations will be useful in deriving the relations for the elastic constants of the nanospring.

2.2. The Kirchhoff rod model

In Kirchhoff's theory, the rod is seen as an assembly of short segments loaded by contact forces from the adjacent segments. The classical equations for the conservation laws of linear and angular momentum are applied to each segment in order to obtain a one-dimensional set of differential equations for the statics and dynamics of the rod in the approximation of large radius of curvature and large total length of the rod as compared to the radius of the local cross section [26]. These equations contain the forces and torques, plus a triad of vectors describing the deformations of the rod. In this paper, we shall be concerned only with static solutions and, therefore, only the static Kirchhoff equations will be presented:

$$\mathbf{F}' = 0, \tag{6}$$

$$\mathbf{M}' + \mathbf{d}_3 \times \mathbf{F} = 0, \tag{7}$$

where $\mathbf{F}$ and $\mathbf{M}$ are the total force and torque across the cross sections of the rod, respectively. $\mathbf{d}_3$ is the vector tangent to the centreline or the axis of the rod. The prime denotes the derivative with respect to the arc-length s of the rod. In order to solve the equations we introduce the constitutive relationship from linear elasticity theory [26] that, for a rod with elliptic cross section, is given by [27]

$$\mathbf{M} = EI_1(k_1 - k_1^{(0)})\mathbf{d}_1 + EI_1a(k_2 - k_2^{(0)})\mathbf{d}_2 + EI_1b(k_3 - k_3^{(0)})\mathbf{d}_3, \tag{8}$$

where E is the Young's modulus, and $a \equiv I_2/I_1$, with I_1 and I_2 being the principal moments of inertia of the cross section in the directions of $\mathbf{d}_1$ and $\mathbf{d}_2$, respectively, with $I_1 \geqslant I_2$. Since the bending coefficient of the rod is proportional to the moment of inertia, the vectors $\mathbf{d}_1$ and $\mathbf{d}_2$ represent the directions of greatest and lowest bending stiffness of the rod, respectively. a, $0 < a \leqslant 1$, measures the bending asymmetry of the cross section. $\mathbf{d}_1$ and $\mathbf{d}_2$ lie in the plane of the cross section, so $\{\mathbf{d}_1, \mathbf{d}_2, \mathbf{d}_3\}$ forms a right-handed director basis defined at each point along the axis of the rod. The constant b is called the *scaled torsional stiffness* and for a rod of elliptic cross section with semiaxes A and B ($A < B$), a and b are given by [27–29]

$$a = \frac{A^2}{B^2}, \qquad b = \frac{1}{1+\sigma}\frac{2a}{1+a}, \tag{9}$$

where σ is the Poisson's ratio of the material.

k_j, $j = 1, 2, 3$, are the components of the so-called *twist vector*, $\mathbf{k}$, which defines the variation of the director basis $\{\mathbf{d}_1, \mathbf{d}_2, \mathbf{d}_3\}$ with the arc-length s through the expression

$$\mathbf{d}_j' = \mathbf{k} \times \mathbf{d}_j, \qquad j = 1, 2, 3. \tag{10}$$

k_1 and k_2 are related to the curvature κ of the centreline of rod through $\kappa = \sqrt{k_1^2 + k_2^2}$, and k_3 is the twist density of the rod. $k_j^{(0)}$, $j = 1, 2, 3$, defines the variation of the director basis of the rod in its unstressed configuration. $k_j^{(0)}$, $j = 1, 2, 3$, represent the *intrinsic curvature* of the rod, which is the tridimensional configuration displayed by the rod when it is free from stresses.

The Kirchhoff equations (6)–(8) admit two types of helical solution for rods with elliptic cross section, called *normal* and *binormal* helices. A helical solution is represented by a set of expressions for the twist vector and the force, and the upper index n (b) will be used to denote *normal* (*binormal*) helical solutions. Figure 2 displays examples of these types of helix. The *normal* helix solution is given by

$$\mathbf{k}^n = \kappa \mathbf{d}_1 + \tau \mathbf{d}_3, \tag{11}$$

$$\mathbf{F}^n = \gamma_1 \tau\, \mathbf{k}^n. \tag{12}$$

The *binormal* helix solution is given by

$$\mathbf{k}^b = \kappa \mathbf{d}_2 + \tau \mathbf{d}_3, \tag{13}$$

$$\mathbf{F}^b = \gamma_2 \tau\, \mathbf{k}^b. \tag{14}$$

where κ (*curvature*) and τ (*torsion*) are the geometric parameters of the space curve defined by the helical axis of the rod, and

$$\gamma_i = b\left(1 - \frac{\tau_0}{\tau}\right) - [1 + (a-1)\delta_{i2}]\left(1 - \frac{\kappa_0}{\kappa}\right), \qquad i = 1, 2 \tag{15}$$

where κ_0 and τ_0 are the *intrinsic* curvature and torsion of the helical structure ($\mathbf{k}^{(0)} = \kappa_0 \mathbf{d}_i + \tau_0 \mathbf{d}_3$), $i = 1$ ($i = 2$) for a *normal* (*binormal*) helix. δ_{i2} is the Kronecker delta.

We can relate the director basis, $\{\mathbf{d}_1, \mathbf{d}_2, \mathbf{d}_3\}$, to the fixed Cartesian basis, $\{\mathbf{e}_x, \mathbf{e}_y, \mathbf{e}_z\}$, integrating equation (10) using

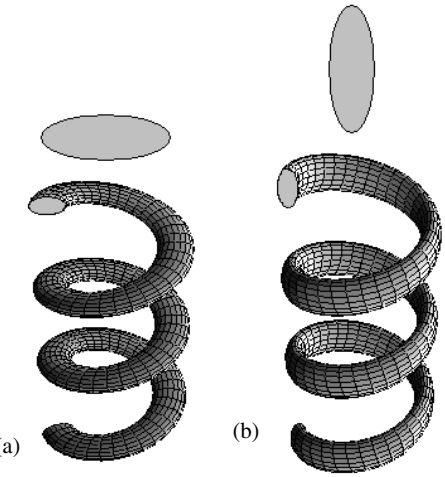

Figure 2. *Normal* (a) and *binormal* (b) helices and the corresponding orientated cross sections.

equations (11) and (13) for *normal* and *binormal* helices, respectively. We obtain the following relations:

$$\mathbf{d}_1^n = \frac{1}{\lambda}(\tau \sin(\lambda s)\mathbf{e}_x - \tau \cos(\lambda s)\mathbf{e}_y + \kappa\, \mathbf{e}_z), \tag{16}$$

$$\mathbf{d}_2^n = \cos(\lambda s)\mathbf{e}_x + \sin(\lambda s)\mathbf{e}_y, \tag{17}$$

$$\mathbf{d}_3^n = \frac{1}{\lambda}(-\kappa \sin(\lambda s)\mathbf{e}_x + \kappa \cos(\lambda s)\mathbf{e}_y + \tau\, \mathbf{e}_z), \tag{18}$$

for the *normal* helix, and

$$\mathbf{d}_1^b = \sin(\lambda s)\mathbf{e}_x + \cos(\lambda s)\mathbf{e}_y, \tag{19}$$

$$\mathbf{d}_2^b = \frac{1}{\lambda}(\tau \cos(\lambda s)\mathbf{e}_x - \tau \sin(\lambda s)\mathbf{e}_y + \kappa\, \mathbf{e}_z), \tag{20}$$

$$\mathbf{d}_3^b = \frac{1}{\lambda}(-\kappa \cos(\lambda s)\mathbf{e}_x + \kappa \sin(\lambda s)\mathbf{e}_y + \tau\, \mathbf{e}_z), \tag{21}$$

for the *binormal* helix. Since $\mathbf{d}_3 = \mathbf{x}'$ we can integrate equations (18) and (21) to obtain an expression for $\mathbf{x}$ similar to equation (4), except for a difference in phase.

From equations (12) and (14) we can obtain the total tension force T along the direction of the axis of the helix (here defined as $\mathbf{e}_z$):

$$T = \mathbf{F} \cdot \mathbf{e}_z = \gamma_i \tau \mathbf{k} \cdot \mathbf{e}_z, \qquad i = 1, 2, \tag{22}$$

where γ_i is given by equation (15) and $i = 1$ ($i = 2$) is related to the vectors $\mathbf{F}$ and $\mathbf{k}$ for the *normal* (*binormal*) helix given by equation (11) (equation (13)). Since the twist vector $\mathbf{k}$ is written in the director basis through equation (11) (equation (13)), we can use equation (16) (equation (19)) to obtain T:

$$T = \frac{EI_1}{L^2}\gamma_i L^2 \tau\, \lambda = EI_1\, \gamma_i\, \tau\, \lambda, \qquad i = 1, 2, \tag{23}$$

where the terms EI_1/L^2 and L^2 appeared in accord to the following conversion to unscaled variables:

$$T \to \frac{L^2}{EI_1}T, \qquad \kappa \to L\kappa, \qquad \tau \to L\tau \qquad \text{and} \qquad \lambda \to L\lambda, \tag{24}$$

with L being a length scale of the rod that, in our case, is chosen to be the arc-length of one loop of the unstressed helical rod: $L = 2\pi/\lambda_0$ with $\lambda_0 = \sqrt{\kappa_0^2 + \tau_0^2}$. E is the Young's modulus of the composite material of the rod, and I_1 is the moment of inertia along $\mathbf{d}_1$ (it is the direction of the greatest bending stiffness). For an elliptic cross section of semiaxes A and B ($A < B$), I_1 is given by

$$I_1 = \frac{B^3 A\pi}{4}. \tag{25}$$

2.3. Expressions for the elastic constants of the nanospring

McMillen and Goriely [23] used the Kirchhoff model to obtain an expression for the Hooke's constant h of a helix, with intrinsic curvature $\mathbf{k}^{(0)} = \kappa_0\mathbf{d}_1 + \tau_0\mathbf{d}_2$, in terms of the properties of the rod's material, the Young's modulus, and the moment of inertia of the circular cross section.

Here, we follow the same steps to derive an expression for the Hooke's constant of a helical filament with elliptic cross section. We also derive an expression relating a torque applied along the direction of the helical axis to the Poisson's ratio of the helical filament.

Consider a helical rod in its unstressed state represented by $\mathbf{k}^{(0)} = \kappa_0\mathbf{d}_i + \tau_0\mathbf{d}_3$, $i = 1$ ($i = 2$) for *normal* (*binormal*) intrinsically helical configuration. The ends of the rod are held fixed so that they do not rotate as the applied tension at the ends is changed. Since the ends do not rotate, this imposes a constraint in the total twist T_W of the rod:

$$T_W \equiv \int k_3\,\mathrm{d}s = \int \tau_0\,\mathrm{d}s = \int \tau\,\mathrm{d}s. \tag{26}$$

The consequence of this constraint is that the torsion τ remains constant ($\tau = \tau_0$) for the tensioned helical rod.

Consider two material points, Q_1 and Q_2, in the unstressed configuration, that are located at arc-length positions $s_1 = 0$ and $s_2 = 2\pi/\lambda_0$, respectively. $2\pi/\lambda_0$ is exactly the arc-length of one loop of the unstressed helical configuration. When a tension is applied to the rod, the distance between those points Q_1 and Q_2, along the helix axis, is given by $d = z(2\pi/\lambda_0) - z(0)$. Using equation (4), d can be written as

$$d = \frac{2\pi\tau}{\lambda\lambda_0}, \tag{27}$$

where λ and τ are related to the deformed (stretched or compressed) helical structure. From (27), we obtain the expression for τ:

$$\tau = \tilde{d}\lambda, \tag{28}$$

where $\tilde{d}$ is the dimensionless distance

$$\tilde{d} \equiv \frac{d}{L} = d\frac{\lambda_0}{2\pi}. \tag{29}$$

The equation (15) can be simplified for this case where $\tau = \tau_0$:

$$\gamma_i = [1 + (a-1)\delta_{i2}]\left(\frac{\kappa_0}{\kappa} - 1\right), \qquad i = 1, 2. \tag{30}$$

Substituting equation (30) in equation (23) we obtain the following expression for the tension T:

$$T = EI_1[1 + (a-1)\delta_{i2}]\left(\frac{\kappa_0}{\kappa} - 1\right)\tau\lambda, \qquad i = 1, 2. \tag{31}$$

From the relation (5), using equation (28), we obtain

$$\kappa = \sqrt{\lambda^2 - \tau^2} = \lambda\sqrt{1 - \tilde{d}^2}. \tag{32}$$

Substituting equation (32) in (31), and using equation (28), we obtain an expression for T as a function of $\tilde{d}$:

$$T = EI_1[1 + (a-1)\delta_{i2}]\left(\frac{\kappa_0\tau}{\sqrt{1-\tilde{d}^2}} - \frac{\tau^2}{\tilde{d}}\right), \qquad i = 1, 2. \tag{33}$$

If $\tilde{d}_0$ is the distance between the points Q_1 and Q_2 in the unstressed configuration of the rod, then $\tilde{d} = \tilde{d}_0 = \tau_0/\lambda_0$ when no tension is applied to the rod. Equation (33) shows that the tension T varies from 0 to ∞ if $\tilde{d}$ varies from $\tilde{d}_0$ to 1. In order to find the Hooke's constant, h, of the tensioned helical rod, we consider a small variation of $\tilde{d}$ defined by the small displacement $\hat{d}$, i.e., we let $\tilde{d} = \tilde{d}_0 + \hat{d}$, $\hat{d} \ll 1$. Then we look for an expression for the Hooke's constant such that

$$T = h\hat{d} + \mathrm{O}(\hat{d}^2). \tag{34}$$

Expanding equation (33) for a small variation of $\tilde{d}$ around $\tilde{d}_0$, we obtain

$$T = EI_1[1 + (a-1)\delta_{i2}]\lambda_0^2\left(1 + \frac{\tau_0^2}{\kappa_0^2}\right)\hat{d} + \mathrm{O}(\hat{d}^2), \qquad i = 1, 2. \tag{35}$$

For a spring with N coils, its displacement due to the action of a given tension T is obtained replacing $\{\hat{d}\}$ by $\{\frac{\hat{d}}{NL}\}$ in the above equation with $\hat{d}$ in unscaled units. It gives the following final expression for the Hooke's constant, h:

$$h = \frac{EI_1}{2\pi N}[1 + (a-1)\delta_{i2}]\lambda_0^3\left(1 + \frac{\tau_0^2}{\kappa_0^2}\right), \qquad i = 1, 2, \tag{36}$$

where $i = 1$ ($i = 2$) refers to the *normal* (*binormal*) helix solution. By making $a = 1$ we recover our previous result [12] for the Hooke's constant of a nanospring made of a nanowire with circular cross section.

Equation (36) relates the Hooke's constant, h, to the Young's modulus, E, of the material composite of the nanospring, to the moment of inertia, I_1, and to the geometric parameters κ_0, τ_0 and $\lambda_0 = \sqrt{\kappa_0^2 + \tau_0^2}$. The moment of inertia, I_1, and the parameter a can be obtained by measuring the semiaxes A and B of the elliptic cross section of the nanowire and using equations (25) and (9), respectively. The geometric parameters can be obtained by measuring the radius, R, and the pitch, P, of the nanospring and using the equations (2) and (3) that relate R and P to λ, κ and τ. To obtain the values of the geometric parameters of the unstressed configuration, we must measure R_0 and P_0 of the unstressed helical configuration, and then use equations (2) and (3) to obtain λ_0, κ_0 and τ_0. Therefore, by measuring the Hooke's constant of the nanospring we can use equation (36) to obtain the Young's modulus of the composite material of the nanospring. Figure 3 shows a scheme that can be used for measuring the Hooke's constant of the nanospring.

We now derive an expression to obtain the Poisson's ratio σ of the nanospring. We depart from equation (8) for the total torque across each cross section, and then use equation (11)

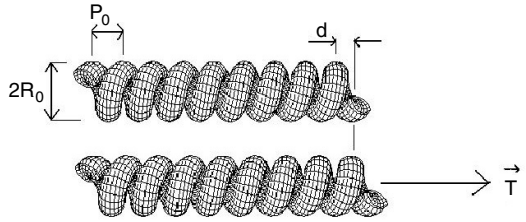

Figure 3. Outline of the experiment to measure the Hooke's constant, h. R_0 and P_0 are the radius and the pitch of the helix in the unstressed configuration. The helix shown corresponds to a nanospring of radius $R_0 = 51$ nm and $P_0 = 85$ nm.

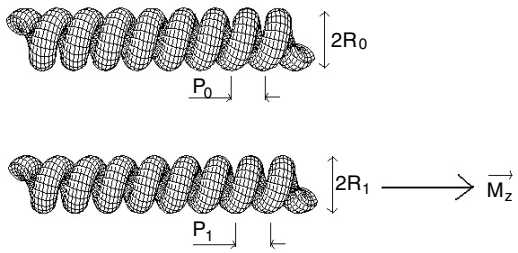

Figure 4. Outline of the experiment to measure the Poisson's ratio σ. The extremities of the nanospring must be held fixed. See the text for details.

(equation (13)) for the components of the twist vector $\mathbf{k}$ for a *normal* (*binormal*) helix. Basically, we want to obtain the axial component of the torque $M_Z \equiv \mathbf{M} \cdot \mathbf{e}_z$. Using equations (16) and (19) we obtain the following expression for M_Z:

$$M_Z = [1 + (a-1)\delta_{i2}](\kappa - \kappa_0)\frac{\kappa}{\lambda} + b(\tau - \tau_0)\frac{\tau}{\lambda}, \quad i = 1, 2, \tag{37}$$

where $i = 1$ ($i = 2$) corresponds to a *normal* (*binormal*) helical nanospring.

Equation (37) can be used to obtain, experimentally, the Poisson's ratio σ of the nanospring. Figure 4 shows a scheme to obtain the Poisson's ratio. Measuring the radius, R_1, and the pitch, P_1, of the stressed helix, κ and τ can be obtained from equations (2) and (3). By measuring the applied torque in the direction of the axis of the helix, M_Z, we can use equation (37) to obtain the parameter b. The values of a, κ_0, τ_0, I_1 and the nanospring Young's modulus are needed to obtain b. The Poisson's ratio, σ, can, therefore, be obtained using equation (9). In this experimental scheme, both ends of the nanospring must be held fixed in order to avoid relaxation.

3. Results and discussions

In this section, we test and discuss the consequences of our model (equations (36) and (37)), and show the importance of the presence of catalytic particles in the growth process of nanosprings.

3.1. Test and discussion of the model

Equation (36) can be tested using the parameters for a unit nanocoil ($N = 1$) considered by Chen *et al* [10]: the diameter of the nanowire $D = 120$ nm, the radius of the helix $R = 420$ nm and the pitch of the helix $P = 2000$ nm. The material has a Poisson's ratio $\sigma = 0.27$ and a shear modulus $\mu = 2.5$ GPa. The amorphous carbon nanocoil used by Chen *et al* is, in fact, a double coil formed by two wires tightly joined [10, 30], as indicated by scanning electron microscope (SEM) and transmission electron microscope (TEM) images depicted in figure 7 of [10]. To test our model, we shall approximate the carbon nanocoil by a homogeneous rod with circular cross section of diameter D.

Assuming that the rod has circular cross section, equation (9) gives $a = 1$ and $b = (1+\sigma)^{-1} = 2\mu/E$. Using the values given above for μ and σ, we obtain that the nanocoil material has the Young's modulus $E_{\text{bulk}} = 6.35$ GPa.

Now, using equations (2) and (3) we obtain κ_0 and τ_0 of the carbon nanocoil from the values of R and P given above. Then, using the measured Hooke's constant of the nanocoil, $h = 0.12$ N m^{-1} [10], equation (36), with $a = 1$ (circular cross section), and $N = 1$ (unit nanocoil), gives $E_{\text{nanocoil}} \simeq 6.88$ GPa, which is slightly larger than $E_{\text{bulk}} = 6.35$ GPa.

This difference cannot be explained by the approximation we made of the nanocoil being a homogeneous rod with circular cross section. In fact, several experimentalists have observed that the measured Young's modulus and Poisson's ratio of nanostructures differ from those of the bulk material. For instance, Salvadori *et al* found that the Young's modulus of gold thin film is about 12% smaller than that of the bulk material [31, 32]. Using alternating electrical fields, Dikin *et al* [33] excited bending vibrations in SiO_2 nanowires to measure their Young's modulus, obtaining values smaller than that of the bulk SiO_2 material. In another example, Cuenot *et al* [34] used the effects of surface tension in bent structures to explain the larger values of the Young's modulus observed in nanowires with smaller diameters. Our model allows us to obtain the Young's modulus and the Poisson's ratio of a helical nanostructure directly; it does not use the bulk material values.

Equation (36) shows that, for a nanowire where $a \neq 1$ (non symmetric cross section, equations (8) and (9)), the Hooke's constant of the *normal* helical configuration is always larger than that of the *binormal* one. It indicates that it is possible to produce helical nanowires whose axes have the same curvature and torsion but different elastic properties (depending on the orientation of the cross section), which is useful in nanoengineering.

Equation (37) cannot be tested due to lack of experimental measurements of the axial torque of a nanospring. However, the recently developed method of measuring axial torque applied to polymers [35] could help the development of experiments to apply axial torques to nanosprings and nanowires. Equation (37) shows that, for a nanowire where $a \neq 1$, the torque required to twist a nanospring is different for *normal* and *binormal* configurations.

3.2. Mechanical function of the catalyst

McIlroy *et al* [1, 6] have proposed a model of nanospring formation based upon the vapour–liquid–solid (VLS) growth mechanism by Wagner and Ellis [14]. The key feature of the VLS model is the presence of a liquid catalyst that absorbs the material from surrounding vapour and, after becoming supersaturated, the material is deposited beneath the catalyst–substrate interface, thereby forming the nanowire [1, 6].

The geometry of the catalyst has a strong influence on the geometry of the growing nanowire and this feature was explored by McIlroy *et al* in their modified VLS growth model for nanosprings [1, 6]. Since the growth is driven by the interaction of the surface tensions between the liquid–vapour (γ_{LV}), solid–vapour (γ_{SV}) and solid–liquid (γ_{SL}) interfaces, they proposed that the asymmetric growth of the nanowire, which leads to the helical shape of the nanostructure, occurs due to the contact angle anisotropy (CAA) at the catalyst–nanowire interface. The work required to shear the catalyst from the nanowire is called the thermodynamic work of adhesion W_A, and it can be computed in terms of the surface tensions by [1]

$$W_A = \gamma_{SV} + \gamma_{SL} - \gamma_{LV} = \gamma_{SV}(1 - \cos\theta), \tag{38}$$

where θ is the angle between the surface tensions γ_{SL} and γ_{SV}.

Goriely and Tabor developed a dynamical method to test the stability of equilibrium solutions of the Kirchhoff model [36, 37], and showed [38] that helices with intrinsic curvature ($\kappa_0 \neq 0$ and $\tau_0 \neq 0$) do not admit unstable modes, being, therefore, dynamically stable. Therefore, *intrinsic curvature* is the key feature for stability of helices and it comes just from the *differential growth* of a one-dimensional structure.

McMillen and Goriely [23] have pointed out that the *differential growth* in tendrils of climbing plants produces *intrinsic curvature*. According to McIlroy's modified VLS model, the CAA at the catalyst–nanowire interface is responsible for the asymmetric growth of the forming helical nanowire. Therefore, the CAA *induces a helical differential growth*, thus producing the *helical intrinsic curvature* required for dynamical stability of the forming nanospring.

The *differential growth* of a helical nanowire is determined by the CAA, which depends on the presence of the catalyst. Therefore, we can conclude that the catalytic particles are responsible for conferring mechanical stability on the nanosprings grown by the VLS growth model. This shows that the McIlroy *et al* VLS growth model is consistent with the mechanical stability of the grown helical nanostructures.

This importance is corroborated by the analysis of a recent report on spontaneous polarization-induced growth of nanosprings and nanorings of piezoelectric zinc oxide (ZnO) by Kong and Wang [5]. Their crystalline nanosprings were produced without the presence of catalytic particles. They found that the mechanism for the formation of the helical structure is the consequence of the interplay between the electrostatic forces between the polarized material and the substrate, and the elastic forces that hold the nanostructure in the helical conformation. If these helical nanostructures were moved away from the substrate, the electrostatic forces would cease and the nanostructure would release its elastic energy, becoming straight, implying that these nanostructures do not have intrinsic helical curvature. The growth process of ZnO nanohelices does not produce *intrinsic curvature*.

Some nanowires grown by chemical vapour deposition (CVD) are not assisted by a *liquid* catalytic particle, indicating that the growth of such nanowires occurs by a vapour–solid–solid (VSS) mechanism [39, 40]. We have given emphasis to the VLS growth mechanism because there are several examples of nanospring growth explained by the VLS mechanism [1, 6–8]. It should be stressed that our analysis can be extended to any type of growth mechanism (including VSS) provided that the growth process presents the geometric features necessary to create the *differential growth*.

4. Conclusions

The Kirchhoff rod model has been used to obtain a simple model for investigating the elastic properties of amorphous nanosprings. We derived the expressions (36) and (37) that can be used to obtain the Young's modulus and the Poisson's ratio of the composite material of a nanospring. These expressions relate the material elastic constants to the geometric features of the nanowire helical structure, and the cross section.

We have considered the case of a nanowire with elliptic cross section that leads to two types of helical solution for the Kirchhoff equations: *normal* and *binormal* helices (figure 2). In the particular case of a nanowire with circular cross section, we recover the expressions derived in [12].

We also proposed the schemes (figures 3 and 4) to be used for measuring the Hooke's constant, and the applied torque along the direction of the axis of the helix, together with the radius, R, and the pitch, P, of the helical structure. Equations (2) and (3) can be used to obtain the curvature, κ, and torsion, τ, of the nanospring, necessary for using equations (36) and (37) to obtain the Young's modulus and the Poisson's ratio of the nanospring.

We have shown that the presence of the catalyst is important for obtaining dynamically stable nanosprings that are grown by the VLS mechanism. We have seen that the *differential growth* produced by the asymmetries in the growth process of a helical nanowire is responsible for the production of its *intrinsic curvature*. We hope that our analysis may stimulate experimentalists to further investigate the growth processes of helical nanostructures.

Acknowledgments

This work was partially supported by the FAPESP, CNPq, IMMP, IN, SAMNBAS and FINEP.

References

[1] McIlroy D N, Alkhateeb A, Zhang D, Aston D E, Marcy A C and Norton M G 2004 *J. Phys.: Condens. Matter* **16** R415
[2] Tang Y H, Zhang Y F, Wang N, Lee C S, Han X D, Bello I and Lee S T 1999 *J. Appl. Phys.* **85** 7981
[3] Zhang H F, Wang C M and Wang L S 2002 *Nano Lett.* **2** 941
[4] Amelinckx S, Zhang X B, Bernaertsm D, Zhang X F, Ivanov V and Nagy J B 1994 *Science* **265** 635
[5] Kong X Y and Wang Z L 2003 *Nano Lett.* **3** 1625
[6] McIlroy D N, Zhang D, Kranov Y and Norton M G 2001 *Appl. Phys. Lett.* **79** 1540
[7] Zhang H F, Wang C M, Buck E C and Wang L S 2003 *Nano Lett.* **3** 577
[8] Zhang D, Alkhateeb A, Han H, Mahmood H, McIlroy D N and Norton M G 2003 *Nano Lett.* **3** 983
[9] Volodin A, Ahlskog M, Seynaeve E, Van Haesendonck C, Fonseca A and Nagy J B 2000 *Phys. Rev. Lett.* **84** 3342

[10] Chen X, Zhang S, Dikin D A, Ding W, Ruoff R S, Pan L and Nakayama Y 2003 *Nano Lett.* **3** 1299
[11] Kirchhoff G 1859 *J. Reine Angew. Math.* **56** 285
[12] da Fonseca A F and Galvao D S 2004 *Phys. Rev. Lett.* **92** 175502
[13] da Fonseca A F, Malta C P and Galvao D S 2006 *J. Appl. Phys.* **99** 094310
[14] Wagner R S and Ellis W C 1964 *Appl. Phys. Lett.* **4** 89
[15] Olson W K 1996 *Curr. Opin. Struct. Biol.* **6** 242
[16] Tobias I, Swigon D and Coleman B D 2000 *Phys. Rev.* E **61** 747
[17] Coleman B D, Swigon D and Tobias I 2000 *Phys. Rev.* E **61** 759
[18] Fonseca A F and de Aguiar M A M 2001 *Phys. Rev.* E **63** 016611
[19] da Fonseca A F and de Aguiar M A M 2003 *Physica* D **181** 53
[20] da Fonseca A F, Malta C P and de Aguiar M A M 2005 *Physica* A **352** 547
[21] Manning R S, Maddocks J H and Kahn J D 1996 *J. Chem. Phys.* **105** 5626
[22] Goriely A and Tabor M 1998 *Phys. Rev. Lett.* **80** 1564
[23] McMillen T and Goriely A 2002 *J. Nonlinear Sci.* **12** 241
[24] Gottlieb O and Perkins N C 1999 *ASME J. Appl. Mech.* **66** 352
[25] Struik D J 1961 *Lectures on Classical Differential Geometry* (Cambridge: Addison-Wesley) p 1
[26] Dill E H 1992 *Arch. Hist. Exact. Sci.* **44** 2
[27] Goriely A and Shipman P 2000 *Phys. Rev.* E **61** 4508
[28] Landau L D and Lifshitz E M 1986 *Theory of Elasticity* (Oxford: Pergamon) p 64
[29] Love A E H 1934 *A Treatise on the Mathematical Theory of Elasticity* (Cambridge: Cambridge University Press) p 317
[30] Huang W M 2005 *Mater. Sci. Eng.* A **408** 136
[31] Salvadori M C, Brown I G, Vaz A R, Melo L L and Cattani M 2003 *Phys. Rev.* B **67** 153404
[32] Salvadori M C, Vaz A R, Melo L L and Cattani M 2003 *Surf. Rev. Lett.* **10** 571
[33] Dikin D A, Chen X, Ding W, Wagner G and Ruoff R S 2003 *J. Appl. Phys.* **93** 226
[34] Cuenot S, Frétigny C, Demoustier-Champagne S and Nysten B 2004 *Phys. Rev.* B **69** 165410
[35] Oroszi L, Galajda P, Kirei H, Bottka S and Ormos P 2006 *Phys. Rev. Lett.* **97** 058301
[36] Goriely A and Tabor M 1996 *Phys. Rev. Lett.* **77** 3537
[37] Goriely A and Tabor M 1997 *Physica* D **105** 20
[38] Goriely A and Tabor M 1997 *Proc. R. Soc.* A **453** 2583
[39] Persson A I, Larsson M W, Stenström S, Ohlsson B J, Samuelson L and Wallenberg L R 2004 *Nat. Mater.* **3** 677
[40] Dick K A, Deppert K, Martensson T, Mandl B, Samuelson L and Seifert W 2005 *Nano Lett.* **4** 761